ISIJ International, Vol. 46 (2006), No. 6, pp. 875–879

Grain Refinement and Improvement in Mechanical Properties of Nb–Al–Si Intermetallic Alloys

Kiyotaka MATSUURA,[1] Dariusz Boleslaw KATA,[2] Jerzy Tadeusz LIS[2] and Masayuki KUDOH[1]

1) Division of Materials Science and Engineering, Hokkaido University, Kita 13 Nishi 8, Sapporo, Hokkaido 060-8628 Japan.
2) Department of Ceramics Technology, AGH University of Science and Technology, Al. Mickiewicza30, 30-059, Cracow, Poland.

(*Received on January 18, 2006; accepted on March 9, 2006*)

Nb–Al–Si intermetallic alloys having submicron crystal grains have been produced using the self-propagating high-temperature synthesis (SHS, or combustion synthesis) method followed by the bead milling technique and the spark plasma sintering (SPS) method. The intermetallic alloys were combustion-synthesized from elemental powders of niobium, aluminum and silicon, and then ball-milled and bead-milled to reduce the alloy powder particle size. The milled alloy powder was consolidated using the SPS method with a sintering time of 300 s at a sintering temperature of 1 373 K. The increase in milling time reduced the grain size of the sintered alloy. Particularly, the grain size was dramatically reduced when zirconia beads of a 0.2-mm diameter were used after milling with zirconia balls of a 10-mm diameter. The Vickers hardness, bending strength and fracture toughness of the sintered alloys increased with the decrease in grain size.

KEY WORDS: powder metallurgy; refractory metal; self-propagating high-temperature synthesis (SHS); spark plasma sintering (SPS); intermetallic compound; niobium.

1. Introduction

Niobium-based alloys have attracted scientists and engineers' attention as new high temperature structural materials, because niobium has an extremely high melting temperature exceeding 2 700 K. There are many reports showing that the mechanical strength and oxidation resistance of the niobium-based alloys at high temperatures can be improved by introducing intermetallic phases into the alloy. According to a study by Tabaru and Hanada,[1] the yield strength and creep rate of Nb–Al alloys dramatically increase with the increase in the volume fraction of Nb_3Al phase. Perkins *et al.*[2] reported that alumina scale formed on the surface of Nb–Al alloys prevents the rapid oxidation. Coating the niobium-based alloys with oxidation resistant intermetallics is also useful for improving the high temperature oxidation behavior. Lee *et al.*[3] studied the high temperature oxidation of a Nb–Al–Si coating sputter-deposited on titanium. Matsuura *et al.*[4] proposed an aluminide coating method based on arc surface alloying of niobium.

Murakami *et al.*[5] studied the mechanical properties and oxidation behaviors of Nb–Al–Si alloys produced by the spark plasma sintering (SPS) of the powder compacts. They reported that an α-based Nb–15Al–25Si alloy (α: $Nb_{10}Al_3Si_3$ intermetallic phase, alloy composition: in molar percent) had a high hardness at room temperature, a high yield stress at 1 573 K and a fair oxidation resistance at 1 573 K, while a β-based Nb–20Al–47Si alloy (β: $Nb_3Al_2Si_5$ intermetallic phase) had a high hardness at room temperature, a low yield stress at 1 573 K and an excellent oxidation resistance at 1 023 and 1 573 K. They found that the excellent oxidation resistance of the β-based alloy was due to the formation of a protective alumina film on its surface.[6]

These studies imply that dual-phase alloys consisting of α and β intermetallic phases may have good combinations of high mechanical strength and excellent oxidation resistance. However, in case of intermetallic compounds such as α- and β-phases, brittleness at room temperature is one of the most significant disadvantages for structural applications.

Schulson and Barker[7] reported that an intermetallic compound of NiAl exhibited a dramatic increase in tensile elongation at 673 K when the grain size was smaller than 10 μm. Their finding implies that intermetallic compounds might exhibit excellent ductility even at room temperature when the grain size is extremely refined to a nanometer order, for example. In this study, the grain size of Nb–Al–Si intermetallic alloys has been reduced to a submicron order, and the effects of the grain refinement on the mechanical properties at room temperature have been investigated.

2. Procedure

Elemental powders of niobium (50 μm in average powder particle diameter and 99.9 wt% in purity), aluminum (100 μm and 99.7 wt%) and silicon (75 μm and 99.999 wt%) were used as the starting materials. They were mixed by hand in a glass beaker using a steel spoon with the addition of a small amount of ethanol. The mixing com-

positions were Nb–50Al–10Si, Nb–40Al–20Si, Nb–30Al–30Si, Nb–25Al–35Si and Nb–34Al–18Si in molar percent. The former four alloys have a niobium concentration of 40 molar percent, while the latter one has a little higher niobium concentration of 48 molar percent. The powder mixture was heated in an alumina crucible in an atmosphere of argon to combustion-synthesize Nb–Al–Si intermetallic alloys. The maximum external heating temperature to trigger off the combustion synthesis (self-propagating high-temperature synthesis, or SHS) reaction was approximately 1 100 K. The external heating rate was approximately 80 K/min.

The synthesized Nb–Al–Si intermetallic alloys were crashed into grains of approximately 1 mm in diameter using a hand hammer in a steel mortar, and then they were ball-milled into powder in a cylindrical zirconia milling vessel of a 15-cm inner diameter and a 15-cm depth using zirconia balls of a 10-mm diameter. The cylindrical milling vessel was horizontally set and was rotated at 50 revolutions per minute on rubber-covered steel rollers. The weight ratio of the intermetallic alloys to the zirconia balls was 1 to 10, and they were placed in the milling vessel of an approximately 2 650-cm^3 volume with the addition of 80 cm^3 of cyclohexane. The ball milling time was varied from 129.6 to 518.4 ks. Some of the ball-milled alloys were additionally bead-milled to reduce the powder particle size more efficiently in a zirconia milling vessel of a 5-cm inner diameter and a 10-cm depth using zirconia beads of a 0.2-mm diameter with cyclohexane. The milling vessel was vertically set and the mixture of the alloy powder and beads was stirred by rotating a zirconia-coated steel impeller at 200 revolutions per minute. The weight ratio of the alloy powder to the beads was 1 to 3, and the volume of cyclohexane used was 80 cm^3. The bead milling time was varied from 3.6 to 36 ks.

The milled alloys were consolidated using the spark plasma sintering (SPS) method. The most significant advantage of the SPS method is prevention of grain growth during sintering, which is brought about due to a low-temperature and short-time sintering. Therefore, it was expected that the grain-refined powder could be consolidated without significant grain growth during sintering. In the present SPS method, the alloy powder was placed in a cylindrical graphite mold having an inner diameter of 30 mm and uniaxially pressed at 60 MPa using graphite punches in vacuum. The SPS temperature and time were 1 373 K and 300 s, respectively. The spark-plasma-sintered sample had a 30-mm diameter and a 5-mm thickness.

An X-ray diffraction (XRD) analysis was performed to identify the phases existing in the sample. Microstructures of the combustion-synthesized and spark-plasma-sintered samples were observed using optical and scanning electron microscopes (OM and SEM), and the phases appearing in the SEM field were identified using an electron probe microanalysis (EPMA). The densities of the combustion-synthesized and spark-plasma-sintered samples were measured using the Archimedes method. The Young's modulus, shear modulus and Poisson's ratio were measured using the ultrasonic method at room temperature. The Vickers hardness test using an applied load of 2 kg, a four-point bending test with a distance between supporting points of 15 mm and a distance between lording points of 4 mm were performed at room temperature. The fracture toughness was evaluated from the crack length of the indentation of the Vickers diamond pyramid based on the JIS R1617 method.

3. Results and Discussion

3.1. Synthesized Intermetallic Alloys

Figure 1 shows a temperature–time curve monitored during heating of an elemental powder mixture having a composition of Nb–40Al–20Si. When the powder mixture was heated to approximately 1 100 K, sudden and dramatic increase in temperature was observed. It was considered that this rapid temperature rise was due to the combustion synthesis reactions between the elemental powders. The XRD analysis performed after cooling revealed that the elemental powder mixture changed into a mixture of $NbAl_3$ and Nb_5Si_3 phases, as shown in **Fig. 2**. Similarly, XRD analyses revealed that all other powder mixtures having different compositions changed into mixtures of intermetallics, as listed in **Table 1**. In all samples investigated in this study, $NbAl_3$ and Nb_5Si_3 phases were detected. In two samples having high silicon contents exceeding 30 molar percent, a niobium alumino-silicide phase of $Nb_3Al_2Si_5$ was also detected. Thus, heating of elemental powder mixtures of niobium, aluminum and silicon leads to the production of mixtures of niobium aluminide, niobium silicide and

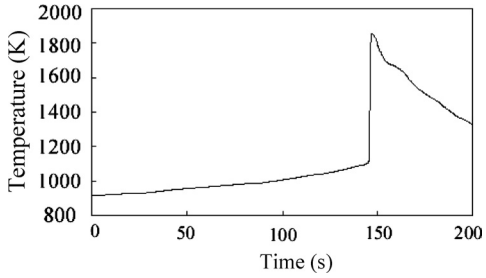

Fig. 1. Change in temperature during heating of a powder mixture having a composition of Nb–40Al–20Si.

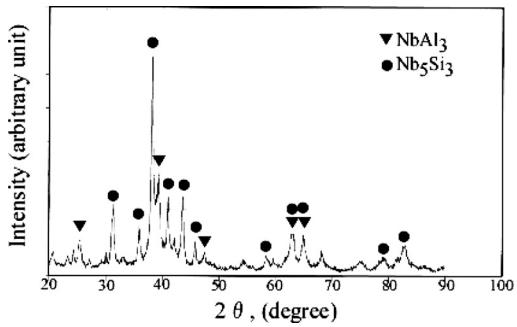

Fig. 2. XRD spectrum of an as-combustion-synthesized sample having a composition of Nb–40Al–20Si.

Table 1. Detected phases in the as-combustion-synthesized samples.

Composition (molar pct)	Detected Phases
Nb-50Al-10Si	$NbAl_3$, Nb_5Si_3
Nb-40Al-20Si	$NbAl_3$, Nb_5Si_3
Nb-30Al-30Si	$NbAl_3$, Nb_5Si_3, $Nb_3Al_2Si_5$
Nb-25Al-35Si	$NbAl_3$, Nb_5Si_3, $Nb_3Al_2Si_5$
Nb-34Al-18Si	$NbAl_3$, Nb_5Si_3

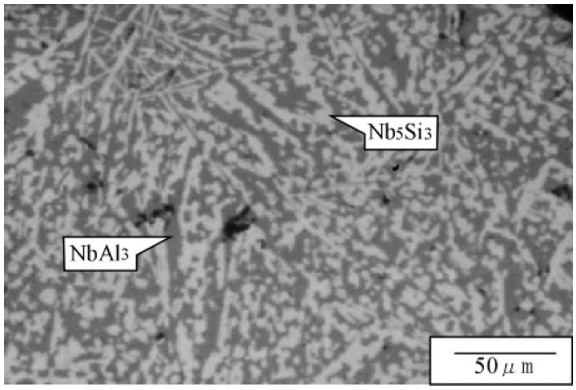

Fig. 3. Microstructure of an as-combustion-synthesized sample having a composition of Nb–40Al–20Si.

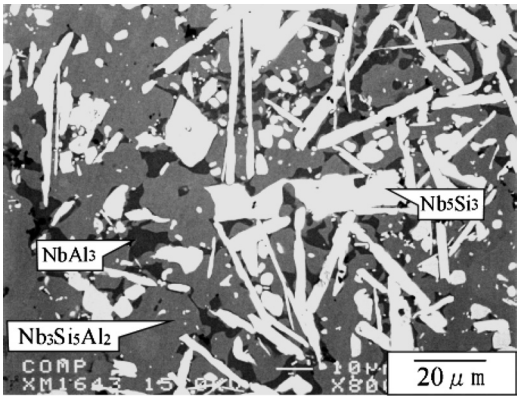

Fig. 4. Microstructure of an as-combustion-synthesized sample having a composition of Nb–25Al–35Si.

niobium alumino-silicide through the combustion synthesis reactions.

Figures 3 and **4** show the microstructures of the as-combustion-synthesized samples having compositions of Nb–40Al–20Si and Nb–25Al–35Si, respectively. In the Nb–40Al–20Si alloy (Fig. 3), a bright rod-like phase is homogeneously distributed in a dark matrix phase. The EPMA revealed that the former was Nb_5Si_3 phase and the latter was $NbAl_3$ phase. The length of the Nb_5Si_3 rods was 10 to 50 μm. In the Nb–25Al–35Si alloy (Fig. 4), on the other hand, although the Nb_5Si_3 rods were similarly distributed, the matrix consisted of $NbAl_3$ and $Nb_3Si_5Al_2$ phases. The $Nb_3Si_5Al_2$ phase had irregular shaped particle morphology with a diameter of 10 to 30 μm. These coarse structures observed in Figs. 3 and 4 imply that they were produced during solidification of the liquid produced due to the combustion synthesis reactions.

The area fractions of these phases were measured using an image analyzer and the results are shown in **Table 2**. For the alloys containing 40% of niobium (upper four alloys in Table 2), as the silicon concentration increased from 10 to 35%, the area fraction of $NbAl_3$ phase decreased from 0.55 to 0.19. On the other hand, the area fraction of Nb_5Si_3 phase increased from 0.45 to 0.58 and then decreased to 0.55 and further to 0.32 as the silicon concentration increased from 10 to 20, 30 and 35%. Also, $Nb_3Al_2Si_5$ phase appeared with an area fraction of 0.16 when the silicon concentration was 30%, and its area fraction increased to 0.49 as the silicon concentration increased to 35%. The alloy containing 48% of niobium (the fifth alloy in Table 2) consisted of $NbAl_3$ and Nb_5Si_3 phases, and the area fraction of Nb_5Si_3 phase was as high as 67%.

Table 2. Area fractions of the constituent phases of the as-combustion-synthesized samples.

Composition (molar pct)	$NbAl_3$	Nb_5Si_3	$Nb_3Al_2Si_5$
Nb-50Al-10Si	0.55	0.45	0
Nb-40Al-20Si	0.42	0.58	0
Nb-30Al-30Si	0.29	0.55	0.16
Nb-25Al-35Si	0.19	0.32	0.49
Nb-34Al-18Si	0.33	0.67	0

Table 3. Density, Vickers hardness and fracture toughness the as-combustion-synthesized samples.

Composition (mol pct)	ρ (Mg/m^3)	HV	K_{IC} ($MPa\,m^{1/2}$)
Nb-50Al-10Si	5.43	820	2.2
Nb-40Al-20Si	5.86	860	2.0
Nb-30Al-30Si	5.29	845	2.0
Nb-25Al-35Si	5.78	840	2.5
Nb-34Al-18Si	5.08	880	2.1

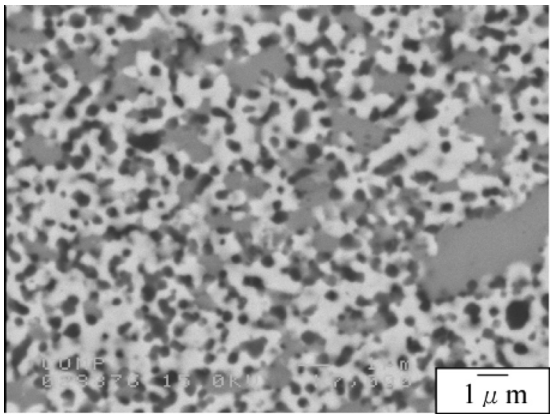

Fig. 5. Microstructure of a sample spark-plasma-sintered after ball milling for 129.6 ks for Nb–40Al–20Si alloy.

All the five different as-combustion-synthesized samples exhibited density of 5.29 to 5.86 g/cm^3, Vickers hardness of 820 to 880 and fracture toughness of 2.0 to 2.5 $MPa\,m^{1/2}$, as shown in **Table 3**. These values do not seem to have any relationship to the compositions of the alloys, but seem to scatter in an experimental error range. The bending strength of the as-combustion-synthesized samples was so low that it could not be measured. The bending specimens were broken when a very light load was applied in the beginning of the bending test. Thus the as-combustion-synthesized samples exhibited a low fracture toughness and poor bending strength, although the hardness was not very low for intermetallic alloys. We have a deep interest in the improvement of these properties due to the grain refinement.

3.2. Milled and Sintered Intermetallic Alloys

The combustion-synthesized samples were crashed into grains, and then the grains were ball-milled into powder, and finally the powder was consolidated into a cylindrical shape using the SPS method. **Figure 5** shows a microstructure observed on a cross-section of a sample spark-plasma-sintered after ball milling for 129.6 ks. The composition of the sample was Nb–40Al–20Si. The microstructure was much finer than that of the as-combustion-synthesized sample shown in Fig. 3. This refinement was attributed to sig-

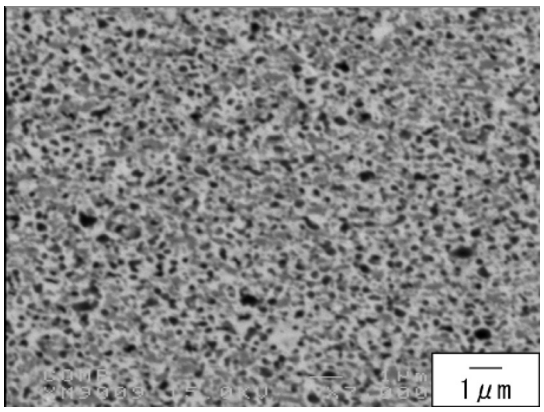

Fig. 6. Microstructure of a sample spark-plasma-sintered after bead milling for 36 ks after ball milling for 129.6 ks for Nb–40Al–20Si alloy.

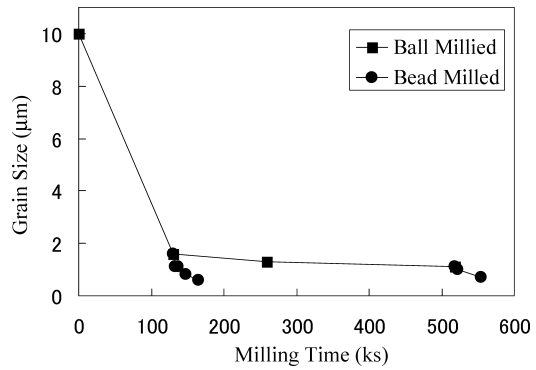

Fig. 7. Effects of milling time on the average grain size for both ball milling and bead milling for Nb–40Al–20Si samples.

nificant grain refinement during the ball milling and less grain growth during the SPS process. **Figure 6** shows a microstructure of a sample spark-plasma-sintered after bead milling for 36 ks after ball milling for 129.6 ks. The bead milling led to further decrease in grain size. This decrease is attributed to an extremely large contact area between the alloy powder and the milling beads.

Figure 7 shows the effect of milling time on the average grain size of the spark-plasma-sintered samples. The average grain size was measured using the intercept method for SEM images of the samples. The grain size dramatically decreased from 10 to 1.6 μm due to ball milling for 129.6 ks. Therefore, it is clear that ball milling is significantly effective in reducing the grain size of the combustion-synthesized intermetallic alloys. However, further increase in ball milling time from 129.6 to 518.4 ks brought about slight decrease in grain size: only 0.5 μm decrease from 1.6 to 1.1 μm, as shown in Fig. 7. It was considered that ball milling with the 10-mm balls was not effective for smaller powder particles because of lower probability of contact between the powder particles and the balls. When 0.2-mm beads were used instead of 10-mm balls, the grain size effectively decreased in a very short milling time, as shown in Fig. 7. Bead milling for 36 ks after ball milling for 129.6 ks brought about a decrease in grain size from 1.6 to 0.6 μm. Similar effect of bead milling was also observed for the powder ball-milled for 518.4 ks. Thus, it was suggested that reducing the ball size brings about an effective reduction in powder particle size during milling.

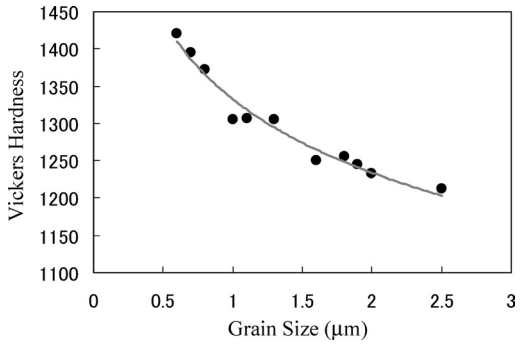

Fig. 8. Relationship between the grain size and the Vickers hardness of the spark-plasma-sintered Nb–40Al–20Si samples.

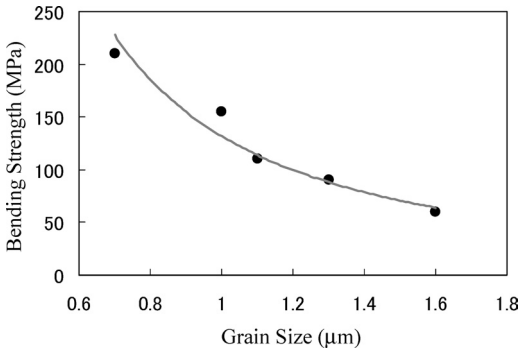

Fig. 9. Relationship between the grain size and the bending strength of the spark-plasma-sintered Nb–40Al–20Si samples.

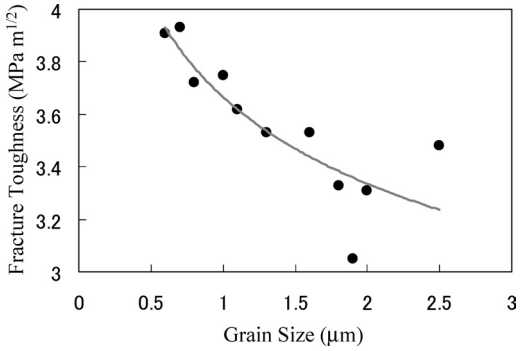

Fig. 10. Relationship between the grain size and the fracture toughness of the spark-plasma-sintered Nb–40Al–20Si samples.

Decrease in grain size brought about increases in Vickers hardness, bending strength and fracture toughness, as shown in **Figs. 8** to **10**. As the grain size decreased from 2.5 to 0.6 μm, the Vickers hardness increased from 1 220 to 1 420, bending strength from 60 to 210 MPa and fracture toughness from 3.2 to 3.9 MPa m$^{1/2}$. Although the fracture toughness values scattered markedly when the grain size was large, the scatter was small when the grain size was small. The Young's modulus, shear modulus and Poisson's ratio of the sample having a grain size of 0.6 μm were 303 GPa, 124 GPa and 0.22, respectively. Murakami *et al.*[6] produced Nb–Al–Si alloys by the SPS process using presintered and ball-milled powders of 325 mesh (~45 μm) in size. They reported Vickers hardness values of 1 200 for a Nb–15Al–25Si alloy and 1 100 for a Nb–20Al–47Si alloy. Although the compositions are different between their al-

loys and the present alloy shown in Fig. 8, the present alloy has higher hardness due to the much finer grain size.

4. Conclusions

Nb–Al–Si intermetallic alloys were combustion-synthesized from the elemental powders and milled using zirconia beads of a 0.2-mm diameter. The milled powder was consolidated using the spark plasma sintering method. The grain size of the sintered sample decreased with the increase in milling time. As the grain size of a Nb–40mol%Al–20mol%Si alloy decreased from 2.5 to 0.6 μm, the Vickers hardness increased from 1 220 to 1 420, bending strength from 60 to 210 MPa and fracture toughness from 3.2 to 3.9 MPa $m^{1/2}$. The Young's modulus, shear modulus and Poisson's ratio of the sample having a grain size of 0.6 μm were 303 GPa, 124 GPa and 0.22, respectively. Thus, grain refinement in niobium-based intermetallic alloys improved the mechanical properties.

Acknowledgement

The authors gratefully acknowledge the financial support of this work by the Grant-in Aid for Scientific Research from Japan Society for the Promotion of Science No. 13650795 and experimental assistance by Mr. K. Taniguchi, a graduate student at Hokkaido University, and Miss R. R. Sanchez, a graduate student at AGH University of Science and Technology.

REFERENCES

1) T. Tabaru and S. Hanada: *Intermetallics*, **6** (1998), 735.
2) R. A. Perkins, K. T. Chiang and G. H. Meier: *Scr. Metall.*, **22** (1988), 419.
3) D. B. Lee, H. Habazaki, A. Kawashima and K. Hashimoto: *Corros. Sci.*, **42** (2000), 721.
4) K. Matsuura, T. Koyanagi, T. Ohmi and M. Kudoh: *Mater. Trans.*, **44** (2003), 861.
5) T. Murakami, S. Sasaki, K. Ichikawa and A. Kitahara: *Intermetallics*, **9** (2001), 621.
6) T. Murakami, S. Sasaki, K. Ichikawa and A. Kitahara: *Intermetallics*, **9** (2001), 629.
7) E. M. Schulson and D. R. Barker: *Scr. Metall.*, **17** (1983), 519.